Electrodeposition of Triangular Pd Rod Nanostructures and Their Electrocatalytic and SERS Activities

Suhee Choi,[†] Hwakyeung Jeong,[†] Kang-hee Choi,[†] Jae Yong Song,*[‡] and Jongwon Kim*[†]

[†]Department of Chemistry, Chungbuk National University, Cheongju, Chungbuk 361-763, Korea
[‡]Center for Nanomaterials Characterization, Korea Research Institute of Standards and Science, Daejeon 305-340, Korea

S *Supporting Information*

ABSTRACT: We report a simple one-step electrodeposition of triangular Pd rod nanostructures on clean Au substrates without additives. Scanning electron microscopy, transmission electron microscopy, and electrochemical techniques were utilized to characterize the structural features of the triangular Pd rod nanostructures. The regulation of the electrodeposition rate by optimizing the electrolyte concentration and applied potential was critical for the anisotropic growth of Pd in the vertical direction. The triangular Pd rod structures exhibited electrocatalytic activities for oxygen reduction and methanol oxidation reactions. These surfaces could be effectively utilized as reproducible surface-enhanced Raman scattering (SERS) active substrates to produce stable SERS signals under electrochemical systems. A simple preparation of well-defined triangular Pd rod structures would allow new opportunities in various areas utilizing Pd-based nanostructured surfaces.

KEYWORDS: *electrodeposition, triangular Pd rod, oxygen reduction, methanol oxidation, surface-enhanced Raman scattering*
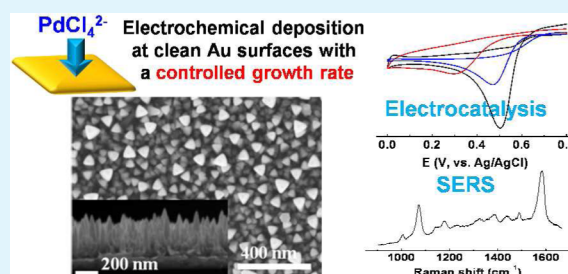
1. INTRODUCTION

Nanostructured metal surfaces have attracted intensive research interest because such surfaces provide useful applications in electrocatalysis, biological labeling, and surface-enhanced Raman scattering (SERS)-based sensing.[1,2] Following the progress in the synthesis of metal nanoparticles of various shapes and sizes, which exhibit unique physical and chemical properties, much attention has recently been paid to assembling nanoparticles on surfaces to construct hierarchical metal nanostructures in order to utilize their unique properties.[3−5] Although assemblies of solution-dispersed metal nanoparticles have been successfully used in diverse applications, the fabrication procedures have multiple steps and are time consuming. Moreover, the linker molecules or capping agents on metal nanoparticles may affect the surface chemistry of the resultant assemblies, which is ultimately not ideal for many applications, particularly electroanalytical ones.[6]

Electrochemical deposition offers an alternative route for the straightforward fabrication of metal surface nanostructures.[7] There have been various efforts to form metal surface nanostructures using electrochemical deposition methods, particularly for Au nanostructures. In many cases, either the pre-modification of substrate electrodes or the addition of additives in the electrolytes is required for the electrodeposition of nanostructured surface architectures.[8] Recently, attention has been focused on the fabrication of nanostructured surfaces by simple electrodeposition on a clean surface without additives or surfactants for use in electrochemical and analytical applications.[9] We have previously reported on the formation of well-defined Au nanostructures by simple electrodeposition methods.[10,11]

Pd has received much attention because of its catalytic activity in heterogeneous reactions and its high hydrogen-storage capability. Particularly, attention has recently been given to the electrocatalytic activity of Pd-based materials in formic acid and methanol oxidation reactions.[12,13] There have been several reports on the electrodeposition of Pd nanostructures. Flower-like Pd nanoparticles were electrodeposited on indium tin oxide (ITO) electrodes modified with thin layers of polymer films.[14] Pd nanodendrites were electrodeposited on glassy carbon (GC) surfaces with the assistance of ethylenediamine as an additive.[15] Recently, Pd nanostructures were electrodeposited on clean surfaces in the absence of additives, including the deposition of nanothorns on carbon surfaces[16,17] and nanodendrites[18] or nanourchins[19] on ITO surfaces.

In the present work, we report a simple electrodeposition of well-defined Pd nanostructures on Au surfaces without additives or pre-modification of the substrate surfaces. Most of the previous work utilized non-metal surfaces such as GC and ITO as the substrates for electrodeposition, whereas we employed Au surfaces as metal substrates to fabricate well-defined rod-type Pd nanostructures with a significantly different morphology from the previously reported Pd structures. The experimental conditions for the formation of these unique Pd

nanostructures, their formation process, and their electro-catalytic and SERS activities were examined.

2. EXPERIMENTAL SECTION

All of the solutions were prepared using purified water (Milli-Q, 18.2 MΩ·cm). K_2PdCl_4 was purchased from Alfa Aesar, and all the other chemicals were purchased from Aldrich. A CHI 600D (CH Instrument) was employed for all the electrochemical measurements. Pt wire and Ag/AgCl electrodes were used as the counter and reference electrodes, respectively. All the potentials were reported relative to the Ag/AgCl reference electrode (3 M NaCl). Au films evaporated onto silicon (Au/Si) wafers (KMAC, Korea) were employed as the substrates for the electrodeposition. After cleaning a Au/Si substrate for 1 min in piranha solution (1:3 by volume of 30% H_2O_2 and H_2SO_4; *Caution: piranha solution reacts violently with most organic materials and must be handled with extreme care*), the substrate was confined in a Viton O-ring with an inner diameter of 2.9 mm and used as a working electrode. Bare Pd and Pt surfaces were prepared from flat Pd plates (Alfa Aesar) and Pt rod electrodes (CH Instrument), respectively, which were mechanically polished with alumina powder from a larger particle size down to the smallest one (ca. 0.05 μm) on a Microcloth pad (Buehler). Electrodeposition was performed in a constant-potential mode using solutions containing K_2PdCl_4 (typically 15 mM for well-defined structures) and 0.1 M H_2SO_4. Scanning electron microscopy (SEM) and transmission electron microscopy (TEM) characterizations were performed using a LEO 1530 field emission SEM (Carl Zeiss) and an aberration-corrected scanning transmission electron microscope (CS-STEM, JEOL ARM200), respectively. The SERS spectra were obtained using a homemade Ramboss micro-Raman system spectrometer equipped with an integral microscope (Olympus BX 51). The 632.8 nm radiation from an air-cooled He/Ne laser was used as an excitation source. The laser power focused on samples was 10 mW.

3. RESULTS AND DISCUSSION

3.1. Electrochemical Deposition of Pd Nanostructures.
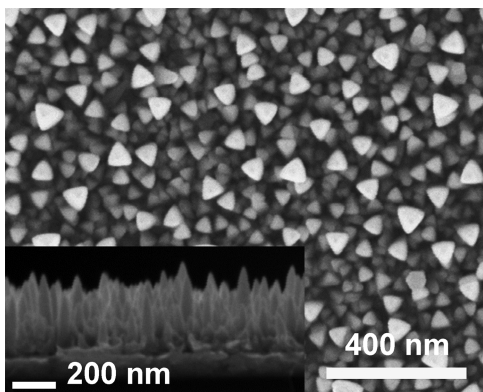Figure 1 shows SEM images of the triangular Pd rod

Figure 1. SEM image of triangular Pd rod structures electrodeposited from solutions containing 15 mM K_2PdCl_4 and 0.1 M H_2SO_4 at −0.1 V with a total deposition charge of 0.02 C. The inset shows a cross-sectional SEM image.

structures electrodeposited on Au surfaces at −0.1 V with a deposition charge of 0.02 C. The dimensions of the triangular Pd rod structures were approximately 100 nm, and the heights ranged from 350 to 400 nm. These structures were homogeneously distributed throughout the entire substrate surface subjected to the electrodeposition (Figure S1, Supporting Information). The Pd nanostructures observed in the present work were unique and significantly different from those previously reported. Most of the Pd nanostructures

previously obtained by electrodeposition were urchin-like particles or dendritic structures, which typically exhibited an isotropic growth in two or three dimensions. In contrast, this triangular Pd rod grew anisotropically in the vertical direction (vide infra for growth pattern).

During the electrodeposition, Pd buffer layers (~90 nm thick) formed on the Au substrate, as shown in the cross-sectional TEM image and STEM energy dispersive spectroscopy (EDS) results (Figure S2, Supporting Information), which agree with the cross-sectional SEM image of Figure 1. In Figure 2A, it is noted that the vertical crystal direction of the Pd buffer
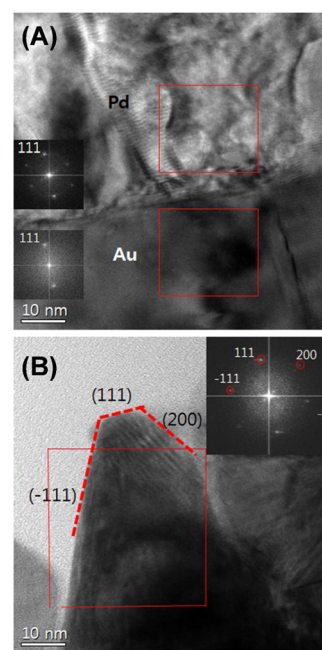

Figure 2. Cross-sectional TEM images of (A) the interface between the Pd buffer layer and Au substrate and (B) the tip of the triangular Pd rod. The insets indicate the fast Fourier transformed images for the areas in the squares.

layer was the [111]-direction, which coincided with the [111]-preferred orientation of the Au layer. This suggests that the epitaxial growth of the Pd might have occurred on the Au substrate, in part, because the lattice spacings of the Au(111) and Pd(111) are similar to each other, with values of 0.2355 and 0.2246 nm, respectively (JCPDS 04-0764 and 46-1043). In addition, the triangular Pd rods grew on the Pd buffer layer in sequence. Figure 2B shows a bright-field TEM image of a tip of triangular Pd rod and fast Fourier transform (FFT) image of the area marked by a red square. The FFT image shows a spot pattern indicating that the triangular Pd rod has a single crystal structure. The appearance of the facets of (111), (-111), and (200) planes also supports that the triangular Pd rod has a single crystal structure. When considering the respective surface energies (0.56, 0.74, and 1.11 eV/atom) of the Pd(111), (100), and (110) planes,[20] it is energetically favorable for the tips of the triangular Pd rods to be surrounded by (111)-facets. However, in the present study, the (100)-facet was partly found, which might be related to the kinetic growth in view of the reduction potential and electrolyte concentration, as will be discussed in the next section.

Triangular Pd rod structures are typically electrodeposited on Au surfaces using a solution containing 15 mM K_2PdCl_4 and

3003

dx.doi.org/10.1021/am405601g | *ACS Appl. Mater. Interfaces* 2014, 6, 3002−3007

0.1 M H_2SO_4 at a constant applied potential of −0.1 V. We examined the effects of the experimental variables during the electrodeposition on the morphology of the Pd deposits. SEM images of Pd structures electrodeposited at various deposition potentials are shown in Figure S3 (Supporting Information). When a deposition potential of −0.2 V was applied, round-shaped Pd deposits with rough surfaces were formed, whereas less-defined sharp Pd protrusions were obtained at 0.0 V. The concentration of K_2PdCl_4 affected the morphology of the Pd deposits (Figure S4, Supporting Information). Lower concentrations of K_2PdCl_4 resulted in Pd deposits with less-defined dendritic structures, whereas higher concentrations of K_2PdCl_4 produced smaller protrusions with sharp edges. To determine the effect of the supporting electrolytes, we performed electrodepositions using solutions containing HCl or $HClO_4$ and obtained the triangular Pd rod structures (Figure S5, Supporting Information), although they were somewhat less defined. Specific adsorption of SO_4^{2-} on Pd surfaces may play a role in the growth of Pd during the electrodeposition,[18] albeit the detailed mechanism is not clear at this stage. However, the typical triangular rod structures were not obtained from solutions with higher pH conditions (Figure S5, Supporting Information). The use of $PdCl_2$ as a precursor produced the triangular rod structures; however, defined Pd rod structures could not be obtained from solutions containing K_2PdCl_6 at various deposition potentials (Figure S6, Supporting Information). This observation implies that the +2 oxidation state of Pd in the precursor compounds is necessary for the formation of triangular Pd rod structures by electrodeposition.

Using optimized electrodeposition conditions for the triangular Pd rod formation, the growth of a triangular rod was investigated by varying the total deposition charge (Figure 3). At an early deposition stage, the deposition current quickly decreased, and then increased up to 0.01 C. The initial current decay is regarded as the double-layer charging process, whereas the subsequent current increase corresponds to the nucleation and growth of the Pd deposits.[21] At this early stage, Pd protrusions were formed on the Au surfaces; the deposition current then remained at a constant level. The triangular structures started to form with a deposition charge of 0.015 C, and well-defined structures were obtained with 0.02 C. The cross-sectional SEM images reveal that the triangular rod structures grew anisotropically in the vertical direction up to a deposition charge of 0.025 C, after which a somewhat larger triangular rod structure appeared. The application of 0.03 C resulted in the dendritic growth of Pd deposits at some point of the triangular rod structures, which continued to grow as uncontrollable dendritic shapes with the further application of the deposition charge.

The results described above suggest that the deposition potential with a proper concentration of K_2PdCl_4 is critical for the formation of well-defined triangular Pd rod structures. The standard reduction potential of $PdCl_4^{2-}(aq)/Pd(s)$ is known to be 0.40 V vs Ag/AgCl,[22] which is significantly more positive than the potential employed for the triangular Pd rod structures, −0.1 V. In this case, the electrodeposition rate for the Pd was mainly affected by the diffusion control; thus, the diffusion limited current at −0.1 V in the cyclic voltammograms became greater as the concentration of K_2PdCl_4 increased (Figure S7A, Supporting Information). During the potentiostatic electrodeposition at −0.1 V, greater steady state currents were recorded at higher K_2PdCl_4 concentrations (Figure S7B, Supporting Information). The steady state currents, reflecting
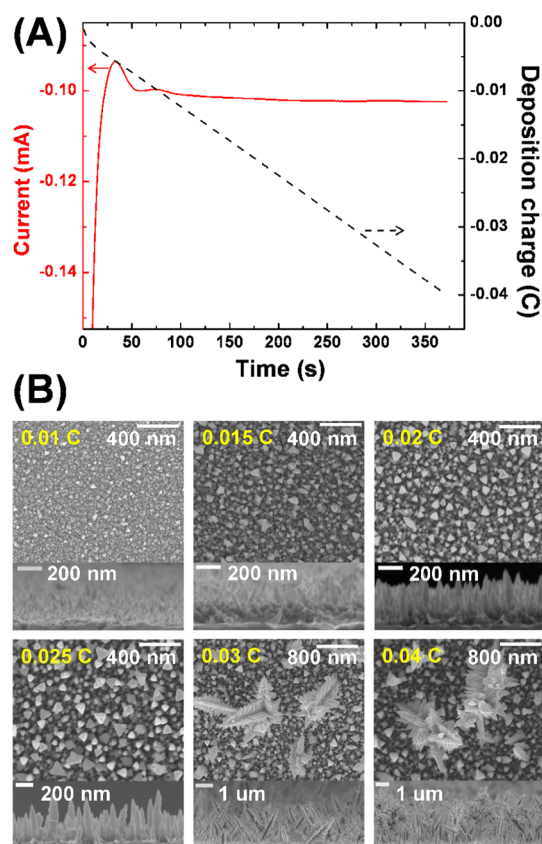

Figure 3. (A) Current and deposition charge vs time curve during electrodeposition in 15 mM K_2PdCl_4 + 0.1 M H_2SO_4 at −0.10 V. (B) Top and cross-sectional SEM images as a function of deposition charge.

the apparent growth rate of the Pd nanostructures during the electrodeposition, therefore depended on both the deposition potential and the concentration of K_2PdCl_4.

The anisotropic growth of Pd in the vertical direction to form triangular Pd rod structures was possible at an optimized electrodeposition rate under appropriate conditions for the concentration and potential. The optimum growth rate is presumed to facilitate the [111]-longitudinal growth of Pd tips surrounded by mainly (111)-facets, as well as partly (100)-facets or higher index planes. It should also be noted that the regulation of the total deposition charge was also important for defined triangular structures. The anisotropic vertical growth of Pd deposits was taken over by a three-dimensional dendritic growth after a critical deposition charge. Once the dendritic Pd deposits formed, the electrodeposition of Pd preferred the dendritic growth to the one-dimensional anisotropic growth, as shown in Figure 3B. In addition, the effects of the substrate on the anisotropic growth of Pd should be noted. It was previously reported that Pd initially formed seed nanoparticles on ITO and GC substrates, and then grew randomly on the seeds. Under the same deposition conditions for triangular Pd rod formation, we observed Pd nanoparticles and dendrites similar to the nanourchin structures reported in the literature.[19] Thus, it is presumed that the formation of a Pd buffer layer epitaxial to the Au substrate played an important role in driving the anisotropic growth at the optimum growth rate.

3.2. Electrocatalytic Activity. The triangular Pd rod surface was characterized using electrochemical methods. The cyclic voltammograms of a triangular Pd rod electrode exhibit

hydrogen adsorption/desorption and Pd oxide formation/reduction peaks in the negative and positive potential regions, respectively, which are characteristically observed on Pd surfaces (Figure S8, Supporting Information). The absence of reduction peaks for the Au oxide (~0.9 V) indicates that the Pd structures cover the entire Au substrate surface. The electrochemical surface area (ESA) of the triangular Pd rod surfaces, which was evaluated by integrating the charge consumed for the reduction of the surface oxide layer,[23] was 0.77 cm^2, which is 2.4 times greater than that of a bare Pd electrode surface (0.31 cm^2). We also evaluated the ESA of the triangular Pd rod surfaces by integrating the charge consumed for the electrooxidation of an adsorbed monolayer of CO (Figure S9, Supporting Information).[24] The ESA of the triangular Pd rod surfaces was 2.6 times greater than that of bare Pd surfaces, which is consistent with the above result.

Another notable feature found in these electrochemical characterizations concerns aspects of the surface orientation of the triangular Pd rod surfaces in contact with electrolyte solutions. The reduction peak of the Pd oxide on the triangular Pd rod surfaces was observed at a potential that was 30 mV more positive than that on bare Pd surfaces (Figure S8, Supporting Information). On the other hand, the stripping waves of CO on the triangular Pd rod surfaces were observed at potential regions that were more negative than those on bare Pd surfaces (Figure S9, Supporting Information). It is known that the reduction peak of Pd oxide shifts to positive potential regions in the order of Pd (111) < Pd (100) < Pd (110), whereas the stripping of CO occurs at more negative potentials in the order of Pd (111) > Pd (110) > Pd (100).[25] Therefore, the electrochemical examination suggested the presence of a significant amount of Pd(110) or Pd(100) crystalline domains on the triangular Pd rod surfaces compared to the bare Pd surfaces. As evidenced by the results of the TEM analysis, the (100)-facet and higher-indexed planes that existed on the surface of the triangular Pd rods were presumed to be related to the electrochemical properties.

The electrocatalytic activity of the triangular Pd rod structures was examined for oxygen reduction reactions, which are important in the development of efficient fuel cell cathodes. Figure 4A compares the cyclic voltammograms obtained on the triangular Pd rod, bare Pd, and Pt surfaces in acidic media. The cathodic peak potential for oxygen reduction on the triangular Pd rod is approximately 200 mV more positive than that on bare Pd surfaces, indicating that the triangular Pd rod surfaces are electrocatalytically active for oxygen reduction. The triangular Pd rod surfaces exhibited a slightly higher electrocatalytic activity than the bare Pt surfaces. The Koutecky−Levich plots obtained from rotating disk electrode measurements (Figure S10, Supporting Information) confirmed that four electrons were associated with the oxygen reduction on the triangular Pd rod surfaces, which is typically observed on Pd surfaces.[26,27] Because Pd(100) is known to be electrocatalytically more active than Pd(111) or Pd(110) for oxygen reduction reactions,[28] the electrocatalytic activity at the triangular Pd rod surfaces can be attributed to the presence of (100)-facets on the Pd surfaces, as evidenced by the electrochemical and TEM examinations.

Methanol oxidation is another important reaction in fuel cell applications. The electrooxidation of methanol on the triangular Pd rod surfaces was examined in basic media, where Pd surfaces exhibit higher electrocatalytic activity for methanol oxidation than in acidic media.[29] Figure 4B shows
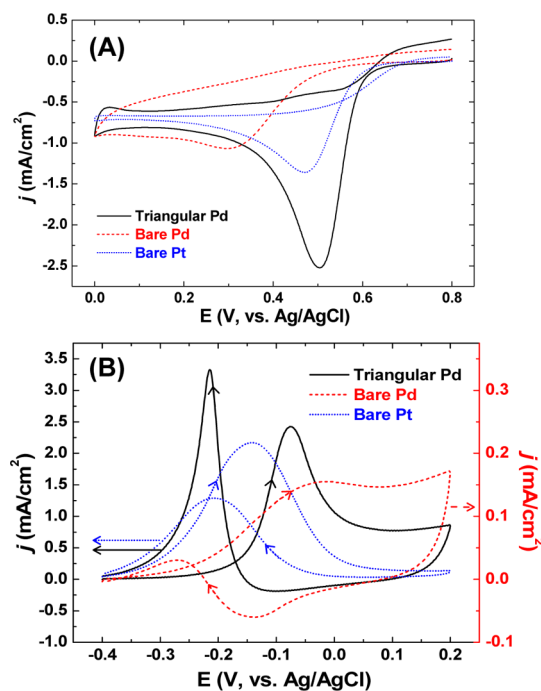

Figure 4. Cyclic voltammograms obtained on bare Pd, bare Pt, and triangular Pd rod surfaces in (A) O_2-saturated 0.1 M $HClO_4$ and (B) 0.1 M methanol + 0.1 M KOH. Scan rate: 50 mV/s.

that a significant increase in the anodic current is measured on a triangular Pd rod compared to bare Pd surfaces. The electrocatalytic activity of triangular Pd rods was similar to that of bare Pt surfaces. The extent of the increase in the anodic current for methanol oxidation on the triangular Pd with respect to the bare Pd surfaces is 7 times larger than that expected from the increase in ESA. It was reported that the Pd crystalline facets have little effect on the activity for the electrooxidation of methanol.[30] Therefore, the high electrocatalytic activity for methanol oxidation on the triangular Pd surfaces might be attributed to the sharp edge sites present on their surfaces. The triangular Pd rod surfaces also exhibited an enhanced electrocatalytic activity for formic acid oxidation (Figure S11, Supporting Information), albeit the enhancement was somewhat lower than that for the methanol oxidation.

3.3. SERS Activity. The unique structural feature of triangular Pd rods suggests that they could be useful as SERS-active substrates. Figure 5A compares the SERS spectra of 4-aminobenzenethiol adsorbed on triangular Pd rod and bare Pd surfaces. The triangular Pd rod surface exhibits a high SERS activity, whereas no detectable signal is observed on the bare Pd surface. The significantly stronger SERS activity observed on the triangular Pd rod surface could be understood in terms of a great increase in the localized electromagnetic field enhancement as a result of the sharp edge sites present on the triangular Pd rod structures.[31,32] We examined how the variation in the SERS intensity depended on the structures of the Pd deposits obtained with different deposition charges (Figure S12, Supporting Information). The Pd deposits obtained with 0.01 C, which lacked well-defined sharp edge sites, exhibited a significantly lower SERS intensity than the triangular Pd rod structures obtained with 0.02 C. The Pd deposits obtained with a higher deposition charge (0.04 C) contained dendritic Pd structures; however, the SERS intensity decreased compared to the triangular Pd rod structures. These results imply that the
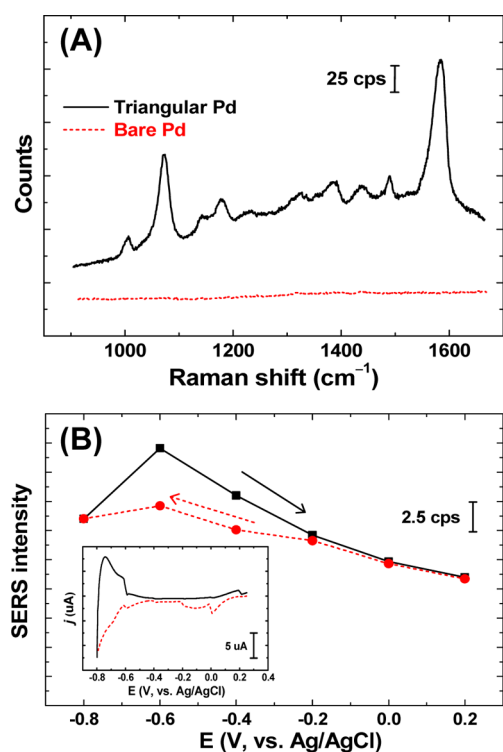
Figure 5. (A) SERS spectra of 4-aminobenzenethiol adsorbed on bare Pd and triangular Pd rod surfaces. The Pd substrates were soaked in 8 mM 4-aminobenzenethiol in ethanol for 12 h and rinsed with ethanol before SERS measurements. The acquisition time was 10 s. (B) Potential dependence of SERS intensity at 1010 cm^{-1} of adsorbed pyridine. Cathodic and anodic sweeps are denoted by circles and squares, respectively. The inset shows the cyclic voltammogram recorded during the SERS measurements.

sharp edge sites on the triangular Pd rod structures significantly contributed to the high SERS activity. To estimate the SERS activity, the SERS enhancement factor (EF) was evaluated using the method developed by Tian et al.[31,33] The SERS EF for the triangular Pd rod structures was calculated to be 4.8 × 10^3, which is comparable to other highly SERS-active Pd nanostructures.[34,35]

In addition to the high SERS activity, the triangular Pd rods exhibited good reproducibility of the SERS intensities, which is a very important characteristic for the application of SERS-active substrates.[36] The spot-to-spot reproducibility in a single triangular Pd rod substrate is shown in Figure S13A (Supporting Information), where the SERS intensities are very uniform. The SERS activities obtained from five different independently fabricated triangular Pd rod substrates were fairly reproducible (Figure S13B, Supporting Information), indicating good substrate-to-substrate reproducibility. This good SERS reproducibility can be attributed to the uniform surface morphology of the triangular Pd rod structures (Figure S1, Supporting Information), which resulted in a homogeneous distribution of the active sites responsible for the SERS enhancement induced by the laser spots.

We also examined the applicability of the triangular Pd rod substrates to electrochemical SERS systems. Figure 5B shows the potential-dependent SERS intensity for the symmetrical ring-breathing mode (~1010 cm^{-1}) from the SER spectra of pyridine adsorbed on the triangular Pd rod surfaces (Figure S14, Supporting Information). The SERS intensities gradually

increased as the electrode potential moved toward the negative region and decreased upon the evolution of hydrogen on the electrode surfaces (inset of Figure 5B). The return of the electrode potential to positive values resulted in bringing the SERS signals back to the original intensities observed before the potential excursion. These results indicate that the triangular Pd rod substrate system is reversible and stable under electrochemical environments. The high SERS activities, as well as the stability upon potential excursions, suggest that the triangular Pd rod substrates can be utilized as electrochemical SERS systems for investigating important electrode reactions on Pd electrode surfaces.

4. CONCLUSIONS

Triangular Pd rod nanostructures were prepared by a simple one-step electrodeposition on clean Au substrates without additives. These triangular Pd rod structures, which were anisotropically grown in the vertical direction on the Au surfaces, were unique in shape compared to other Pd nanostructures that have been electrodeposited on ITO or GC substrates. An optimized rate of electrodeposition under appropriate concentration and potential conditions was important for the anisotropic growth of Pd in the vertical direction to form the triangular Pd rod structures. The triangular Pd rod structures were electrocatalytically active for oxygen reduction and methanol oxidation reactions. These surfaces also exhibited a high SERS activity and can be effectively utilized in electrochemical SERS systems. The straightforward preparation method for these well-defined triangular Pd rod structures will provide new opportunities for the utilization of Pd-based substrates in electroanalytical and SERS applications.

■ ASSOCIATED CONTENT

Ⓢ Supporting Information

Additional SEM and TEM images, EDX spectrum, and cyclic voltammograms as noted in the text. This material is available free of charge via the Internet at http://pubs.acs.org.

■ AUTHOR INFORMATION

Corresponding Authors
*E-mail: jysong@kriss.re.kr.
*E-mail: jongwonkim@chungbuk.ac.kr.
Notes
The authors declare no competing financial interest.

■ ACKNOWLEDGMENTS

■ REFERENCES

(1) Solla-Gullon, J.; Vidal-Iglesias, F. J.; Feliu, J. M. Shape Dependent Electrocatalysis. *Annu. Rep. Prog. Chem., Sect. C: Phys. Chem.* **2011**, *107*, 263−297.

(2) Banholzer, M. J.; Millstone, J. E.; Qin, L. D.; Mirkin, C. A. Rationally Designed Nanostructures for Surface-Enhanced Raman Spectroscopy. *Chem. Soc. Rev.* **2008**, *37*, 885−897.

(3) Shipway, A. N.; Katz, E.; Willner, I. Nanoparticle Arrays on Surfaces for Electronic, Optical, and Sensor Applications. *ChemPhysChem* **2000**, *1*, 18−52.

(4) Velev, O. D.; Gupta, S. Materials Fabricated by Micro- and Nanoparticle Assembly - the Challenging Path from Science to Engineering. *Adv. Mater.* **2009**, *21*, 1897−1905.

(5) Wang, L. B.; Xu, L. G.; Kuang, H.; Xu, C. L.; Kotov, N. A. Dynamic Nanoparticle Assemblies. *Acc. Chem. Res.* **2012**, *45*, 1916−1926.

(6) Shenhar, R.; Norsten, T. B.; Rotello, V. M. Polymer-Mediated Nanoparticle Assembly: Structural Control and Applications. *Adv. Mater.* **2005**, *17*, 657−669.

(7) Bicelli, L. P.; Bozzini, B.; Mele, C.; D'Urzo, L. A Review of Nanostructural Aspects of Metal Electrodeposition. *Int. J. Electrochem. Sci.* **2008**, *3*, 356−408.

(8) Bartlett, P. N.; Baumberg, J. J.; Coyle, S.; Abdelsalam, M. E. Optical Properties of Nanostructured Metal Films. *Faraday Discuss.* **2004**, *125*, 117−132.

(9) Guo, S.; Wang, L.; Wang, E. Templateless, Surfactantless, Simple Electrochemical Route to Rapid Synthesis of Diameter-Controlled 3D Flowerlike Gold Microstructure with "Clean" Surface. *Chem. Commun.* **2007**, 3163−3165.

(10) Seo, B.; Choi, S.; Kim, J. Simple Electrochemical Deposition of Au Nanoplates from Au(I) Cyanide Complexes and Their Electrocatalytic Activities. *ACS Appl. Mater. Interfaces* **2011**, *3*, 441−446.

(11) Hyun, M.; Choi, S.; Lee, Y. W.; Kwon, S. H.; Han, S. W.; Kim, J. Simple Electrodeposition of Dendritic Au Rods from Sulfite-Based Au(I) Electrolytes with High Electrocatalytic and SERS Activities. *Electroanalysis* **2011**, *23*, 2030−2035.

(12) Zhou, W. P.; Lewera, A.; Larsen, R.; Masel, R. I.; Bagus, P. S.; Wieckowski, A. Size Effects in Electronic and Catalytic Properties of Unsupported Palladium Nanoparticles in Electrooxidation of Formic Acid. *J. Phys. Chem. B* **2006**, *110*, 13393−13398.

(13) Tian, N.; Zhou, Z.-Y.; Yu, N.-F.; Wang, L.-Y.; Sun, S.-G. Direct Electrodeposition of Tetrahexahedral Pd Nanocrystals with High-Index Facets and High Catalytic Activity for Ethanol Electrooxidation. *J. Am. Chem. Soc.* **2010**, *132*, 7580−7581.

(14) Li, Y.; Lu, G.; Wu, X.; Shi, G. Electrochemical Fabrication of Two-Dimensional Palladium Nanostructures as Substrates for Surface Enhanced Raman Scattering. *J. Phys. Chem. B* **2006**, *110*, 24585−24592.

(15) Wang, A.-J.; Li, F.-F.; Bai, Z.; Feng, J.-J. Large-Scale Electrosynthesis of Pd Nanodendrites and Their Improved Electrocatalytic Properties for Methanol Oxidation. *Electrochim. Acta* **2012**, *85*, 685−692.

(16) Meng, H.; Sun, S.; Masse, J.-P.; Dodelet, J.-P. Electrosynthesis of Pd Single-Crystal Nanothorns and Their Application in the Oxidation of Formic Acid. *Chem. Mater.* **2008**, *20*, 6998−7002.

(17) Meng, H.; Xie, F.; Chen, J.; Shen, P. K. Electrodeposited Palladium Nanostructure as Novel Anode for Direct Formic Acid Fuel Cell. *J. Mater. Chem.* **2011**, *21*, 11352−11358.

(18) Song, Y.-J.; Kim, J.-Y.; Park, K.-W. Synthesis of Pd Dendritic Nanowires by Electrochemical Deposition. *Cryst. Growth Des.* **2008**, *9*, 505−507.

(19) Fang, Y.; Guo, S.; Zhu, C.; Dong, S.; Wang, E. Twenty Second Synthesis of Pd Nanourchins with High Electrochemical Activity through an Electrochemical Route. *Langmuir* **2010**, *26*, 17816−17820.

(20) Singh-Miller, N. E.; Marzari, N. Surface Energies, Work Functions, and Surface Relaxations of Low-Index Metallic Surfaces from First Principles. *Phys. Rev. B* **2009**, *80*, 235407.

(21) Martín, H.; Carro, P.; Hernández Creus, A.; González, S.; Salvarezza, R. C.; Arvia, A. J. Growth Mode Transition Involving a Potential-Dependent Isotropic to Anisotropic Surface Atom Diffusion Change. Gold Electrodeposition on HOPG Followed by Stm. *Langmuir* **1997**, *13*, 100−110.

(22) Bard, A. J.; Parsons, R; Jordan, J. *Standard Potentials in Aqueous Solution*; Marcel Dekker: New York, 1985.

(23) Xiao, L.; Zhuang, L.; Liu, Y.; Lu, J. T.; Abruna, H. D. Activating Pd by Morphology Tailoring for Oxygen Reduction. *J. Am. Chem. Soc.* **2009**, *131*, 602−608.

(24) van der Vliet, D. F.; Wang, C.; Li, D. G.; Paulikas, A. P.; Greeley, J.; Rankin, R. B.; Strmcnik, D.; Tripkovic, D.; Markovic, N. M.; Stamenkovic, V. R. Unique Electrochemical Adsorption Properties of Pt-Skin Surfaces. *Angew. Chem., Int. Ed.* **2012**, *51*, 3139−3142.

(25) Hara, M.; Linke, U.; Wandlowski, T. Preparation and Electrochemical Characterization of Palladium Single Crystal Electrodes in 0.1 M H_2SO_4 and $HClO_4$: Part I. Low-Index Phases. *Electrochim. Acta* **2007**, *52*, 5733−5748.

(26) Salvador-Pascual, J. J.; Citalan-Cigarroa, S.; Solorza-Feria, O. Kinetics of Oxygen Reduction Reaction on Nanosized Pd Electrocatalyst in Acid Media. *J. Power Sources* **2007**, *172*, 229−234.

(27) Erikson, H.; Kasikov, A.; Johans, C.; Kontturi, K.; Tammeveski, K.; Sarapuu, A. Oxygen Reduction on Nafion-Coated Thin-Film Palladium Electrodes. *J. Electroanal. Chem.* **2011**, *652*, 1−7.

(28) Shao, M. Palladium-Based Electrocatalysts for Hydrogen Oxidation and Oxygen Reduction Reactions. *J. Power Sources* **2011**, *196*, 2433−2444.

(29) Yang, Y.-Y.; Ren, J.; Zhang, H.-X.; Zhou, Z.-Y.; Sun, S.-G.; Cai, W.-B. Infrared Spectroelectrochemical Study of Dissociation and Oxidation of Methanol at a Palladium Electrode in Alkaline Solution. *Langmuir* **2013**, *29*, 1709−1716.

(30) Ferrin, P.; Mavrikakis, M. Structure Sensitivity of Methanol Electrooxidation on Transition Metals. *J. Am. Chem. Soc.* **2009**, *131*, 14381−14389.

(31) Choi, S.; Ahn, M.; Kim, J. Highly Reproducible Surface-Enhanced Raman Scattering-Active Au Nanostructures Prepared by Simple Electrodeposition: Origin of Surface-Enhanced Raman Scattering Activity and Applications as Electrochemical Substrates. *Anal. Chim. Acta* **2013**, *779*, 1−7.

(32) Jeong, G. H.; Lee, Y. W.; Kim, M.; Han, S. W. High-Yield Synthesis of Multi-Branched Gold Nanoparticles and Their Surface-Enhanced Raman Scattering Properties. *J. Colloid Interface Sci.* **2009**, *329*, 97−102.

(33) Cai, W. B.; Ren, B.; Li, X. Q.; She, C. X.; Liu, F. M.; Cai, X. W.; Tian, Z. Q. Investigation of Surface-Enhanced Raman Scattering from Platinum Electrodes Using a Confocal Raman Microscope: Dependence of Surface Roughening Pretreatment. *Surf. Sci.* **1998**, *406*, 9−22.

(34) Abdelsalam, M. E.; Mahajan, S.; Bartlett, P. N.; Baumberg, J. J.; Russell, A. E. SERS at Structured Palladium and Platinum Surfaces. *J. Am. Chem. Soc.* **2007**, *129*, 7399−7406.

(35) McLellan, J. M.; Xiong, Y.; Hu, M.; Xia, Y. Surface-Enhanced Raman Scattering of 4-Mercaptopyridine on Thin Films of Nanoscale Pd Cubes, Boxes, and Cages. *Chem. Phys. Lett.* **2006**, *417*, 230−234.

(36) Natan, M. J. Concluding Remarks - Surface Enhanced Raman Scattering. *Faraday Discuss.* **2006**, *132*, 321−328.

3007

dx.doi.org/10.1021/am405601g | *ACS Appl. Mater. Interfaces* 2014, 6, 3002−3007